Use of the Abdominal Aorta for Arterial Input Function Determination in Hepatic and Renal PET Studies

Guido Germano, Benjamin C. Chen, Sung-Cheng Huang, Sanjiv S. Gambhir, Edward J. Hoffman, and Michael E. Phelps

Division of Nuclear Medicine and Biophysics, Department of Radiological Sciences, UCLA School of Medicine, Los Angeles, California and Istituto "Fondazione Senatore Pascale," Napoli, Italy

A method using the activity in the abdominal aorta of human and animal subjects to noninvasively estimate blood-pool input function in dynamic, abdominal PET scans is proposed and validated in this paper. Partial volume effects due to the aorta's dimensions are corrected by a semi-automated algorithm based on the transaxial resolution in the reconstructed images. The technique was validated by comparing PET measurements of abdominal aortic activity to well counter measurements of arterial blood samples (eight canine renal studies) and to PET measurements of left ventricular cavity activity (eight human hepatic studies). In renal studies, correlation analysis of the areas subtended by the two input functions yielded an essentially unitary slope (1.03 ± 0.09), with high correlation ($R^2 > 0.95$, $p < 0.001$). In hepatic studies, similar values (0.99 ± 0.03 and $R^2 > 0.85$, $p < 0.001$) were found. Correlation of the blood flow estimates based on the two input functions and a two-compartment model produced slopes of 1.07 ± 0.16 and 1.03 ± 0.07, and correlations of ($R^2 > 0.98$, $p < 0.001$) and ($R^2 > 0.97$, $p < 0.001$) for the renal and hepatic studies, respectively. We conclude that noninvasive, accurate measurements of the arterial input function by dynamic PET imaging are possible and represent a clinically viable alternative to arterial blood sampling.

J Nucl Med 1992; 33:613-620

Positron emission tomography (PET) allows the quantitative measurement of the concentration of positron-emitting tracers within a three-dimensional object in vivo. Through the application of the appropriate mathematical model, such quantitative measurement can be related to a physiologic or biochemical process, which in turn may provide insight into the pathophysiology of disease processes. In order to apply a tracer kinetic model to PET data, it is generally necessary to obtain a blood-pool time-activity curve or input function, which describes the amount and time course of tracer delivered by blood to the organ of interest (*1*). The traditional method of measuring input function in dynamic PET studies is through arterial catheterization followed by blood sampling. Such a procedure is both invasive and cumbersome, making it undesirable for clinical applications (*2*).

In dynamic PET cardiac studies, noninvasive determination of the input function from region of interest analysis (ROI) of the activity in the left ventricular cavity (LVC) has been proposed and validated (*3*). This technique, when used with appropriate corrections for spillover and partial volume effects, yields input functions that correlate well with those obtained through blood sampling (*4*). It has been proposed that a small, dedicated PET tomograph could be used to estimate the arterial input function from the radial artery in human subjects (*5*). This requires the acquisition of a second PET system, a calibration factor between the main and the auxiliary tomograph, and the small size of the radial artery may cause inaccuracies because of the large correction for the partial volume effect.

Recently PET studies have begun to target organs, such as the liver and kidneys, not traditionally associated with PET (*6-9*). In most of these studies, the left ventricular cavity is not included in the field of view (FOV); thus, quantitative analysis of the data would require arterial blood sampling. A fortunate aspect of these studies is that the abdominal aorta is seen in several planes of the data set, and can be used for arterial input function determination. A combination of venous blood sampling and abdominal aorta dynamic PET data has been previously utilized for input function determination (*10*); that method is still invasive, and does not rigorously address the issue of partial volume effects in the aorta.

In this paper, we test the accuracy of a method to determine arterial input function from reconstructed images of the abdominal aorta of animal and human subjects in dynamic PET studies of the kidneys and liver. Partial volume effects causing underestimation of true activity in the aorta are corrected by estimating the diameter of the vessel via activity profile analysis with non-linear regression techniques. In addition, the dependence of the final

Received Jun. 14, 1991; revision accepted Oct. 8, 1991.

For reprints contact: Guido Germano, PhD, Director, Nuclear Medicine Physics, Cedars-Sinai Medical Center A047 N, 8700 Beverly Blvd., Los Angeles, CA 90048.

recovery coefficient on the filter used in the image reconstruction process is determined analytically. Validation of the technique is performed by comparing the corrected abdominal aortic input function to the activity curves obtained independently from PET images of the LVC and from arterial blood sampling. Finally, estimates of tissue blood flow, which were obtained using the abdominal aorta, the LVC and the arterial blood sampling method, are calculated and compared.

THEORY

It is well known that the recovery coefficient (RC) for an object imaged in a PET scanner depends on the size of the object as well as on the resolution of the scanner (*11*). While the latest generation of PET scanners has achieved resolutions close to the theoretical limits for PET (*12,13*), sensitivity and noise considerations still require the use of relatively smooth filters for image reconstruction in most animal and patient studies, and correction factors for partial volume effects must be calculated and applied to structures of interest. Figure 1 shows the transaxial image resolution for a whole-body PET scanner (CTI/Siemens ECAT 931/08) and a Shepp-Logan filter used in image reconstruction as a function of the cutoff frequency.

Let us define the measured concentration C_m at the center of the aorta as the product of the actual concentration C (uniform within the aorta) and the recovery coefficient RC_{aorta}

$$C_m = RC_{aorta} \cdot C. \qquad \text{Eq. 1}$$

If one assumes the section of the abdominal aorta in the plane of interest is a circular structure of radius R (two-dimensional geometry) containing uniform activity, then the recovery coefficient RC_{aorta} can be expressed as the fraction of the volume of a two-dimensional Gaussian (centered on the aorta) that falls within R of the center of the aorta (*14*):

$$RC_{aorta} = 1 - e^{-\frac{R^2}{2s^2}}, \qquad \text{Eq. 2}$$

where s is related to the image resolution (FWHM) by

$$s = \frac{FWHM}{2.355} \qquad \text{Eq. 3}$$

and therefore depends upon the reconstruction filter as shown in Figure 1.

Equation 2 can be utilized directly only if the actual radius of the aorta is known through other procedures (e.g., CT or MRI studies). Given the substantial dependence of the vessel's dimensions on some pathological states (*15*) and their range of variability in the normal patient population, average population dimensions are not a viable option. Furthermore, underlying assumptions can be identified as follows:

1. The aorta section in the plane of interest must have circular shape, i.e., the transaxial image planes must be approximately perpendicular to the aorta's axis. This is a reasonable assumption in view of the anatomical pathway of the abdominal aorta, as well as the fact that current study acquisition protocols do not require tilting of the tomograph's gantry. However, in cases where positioning was not accurate or the aorta section in the image plane is otherwise noncircular, image reslicing may be needed (*16,17*).
2. Equation 1 assumes no spillover from adjacent structures into the aorta. For example, in renal studies the abdominal aorta must be reasonably isolated from the renal cortices. This should be no problem in early images before significant activity has been delivered to the target organs. The high contrast of the aorta effectively isolates it from spillover. At later imaging times the aorta must be sufficiently isolated to allow reasonable estimation and subtraction of background.
3. The final correction for the partial volume effect depends not only on RC_{aorta}, but also on the accuracy of the calculation of C_m in Equation 1. This in turn depends on the size (relative to the aorta) and location of the ROI used for the calculation of C_m. For the best accuracy, small ROIs (2–3 mm in diameter, or less than 1/5 of the aorta's diameter) centered on the pixel of maximum activity in the aorta should be used (*18*).
4. For accurate determination of time-activity curves via ROIs centered on the abdominal aorta, the aorta must not move over the duration of the dynamic study. While this is not a problem in the case of anesthetized animals, in patient studies even a shift

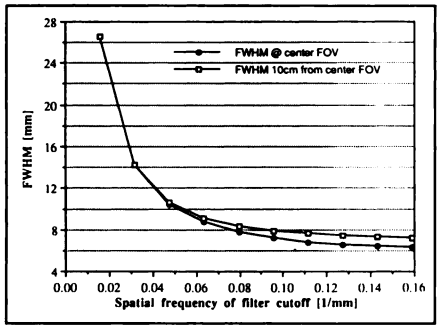

FIGURE 1. Transaxial system resolution for a CTI/Siemens ECAT 931/08 whole-body PET scanner, calculated with a 1-mm diameter, ^{22}Na line source positioned at the center of the FOV and then 10 cm off center. The two sets of images were reconstructed with a Shepp-Logan filter and cutoffs of 10%, 20% ... 100% of the Nyquist frequency, which for this system is 0.159 mm^{-1}.

of a few millimeters may cause a large variation in the value of the measured activity C_m. With regard to this problem, it may sometimes be necessary to manually position the ROIs on the individual dynamic frames for an image plane, as opposed to simply copying the ROI coordinates from one frame to the others.

Even when all of the above assumptions are satisfied, information on the exact diameter of the aorta is in practice often difficult or inconvenient to obtain. It is however possible to estimate it from the PET image through non-linear fitting of an activity profile measured across the aorta, whose circular transaxial section will be now treated as an infinitely long bar of diameter 2R containing true uniform activity C. If the bar is centered on the origin of the x-axis, the measured profile P(x) through the bar is given by:

$$P(x) = \frac{C}{\sqrt{2\pi s^2}} \int_{-R}^{R} e^{\frac{-(x-x_0)^2}{2s^2}} dx_0 = \frac{C}{2}\left(ERF\left(\frac{x+R}{\sqrt{2}s}\right) - ERF\left(\frac{x-R}{\sqrt{2}s}\right)\right), \quad \text{Eq. 4}$$

where C is again the actual activity concentration in the aorta, ERF is the error function

$$ERF(u) = \frac{2}{\sqrt{\pi}} \int_0^u e^{-t^2} dt \quad \text{Eq. 5}$$

and s has the same meaning as in Equation 3. A complete derivation and discussion of this result has been presented previously (*18*). For a narrow strip through the center of the aorta, Equation 4 is a reasonably accurate description of that profile. If a wide strip is chosen, the circular character of the aorta's section becomes a factor and Equation 4 is a poorer approximation to the data. The activity profiles across various bars (4–32 mm in diameter) containing a uniform distribution of activity, as predicted by Equation 4, are shown in Figure 2.

After fitting the measured profile P(x) to Equation 4 to determine C and R, RC_{aorta} can be estimated by substituting the estimate for R in Equation 2. Note that although R is estimated by approximating the profile through the circular aorta section to the profile through a bar, RC_{aorta} is accurately approximated only by using the estimation of recovery of activity from a circular object (Equation 2). The equation that calculates the recovery coefficient for a bar

$$RC_{aorta} = \frac{C_m}{C} \quad \text{Eq. 6}$$

cannot be used because the recovery coefficient for a circular object is only well approximated by the recovery coefficient for a bar for very large (non physiological) circular diameters.

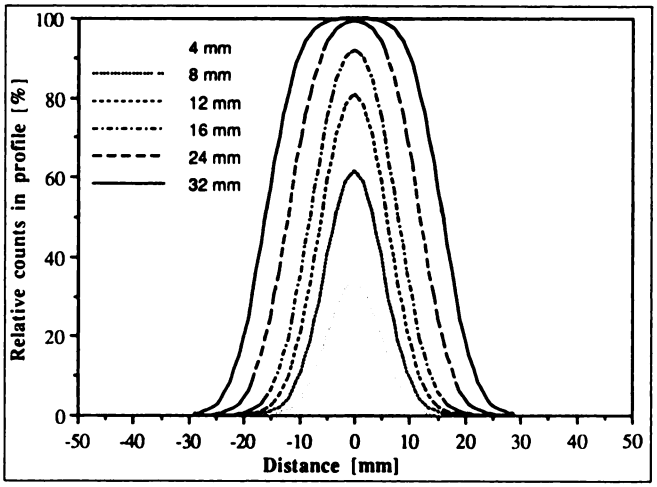

FIGURE 2. Predicted activity profiles across various cylinders (4–32 mm in diameter) containing a uniform distribution of activity. The circular transaxial section of the cylinder is treated as an infinitely long bar centered on the x-axis, and all profiles are calculated from Equation 4. Note that although R is estimated by approximating the profile through the circular aorta section to the profile through a bar, RC_{aorta} is accurately approximated only by using the estimation of recovery of activity from a circular object (Eq. 2). The equation that calculates the recovery coefficient for a bar (Eq. 6) cannot be used because the recovery coefficient for a circular object is only well approximated by the recovery coefficient for a bar for very large (non-physiological) circular diameters.

MATERIALS AND METHODS

Canine Renal Studies

A total of eight dynamic, ^{13}N-ammonia renal PET studies were performed on four mongrel dogs with normal as well as artificially induced low and high flow conditions (*19*). The dogs were positioned laterally in an ECAT 931/08 whole-body PET scanner (CTI/Siemens), with the positioning laser crosshair centered about 10 cm above the lowest rib to ensure the kidneys were in the FOV. Five to 10 mCi of ^{13}N-ammonia were injected intravenously over 30 sec for each study. The scan protocol consisted of twelve 10-sec frames and six 20-sec frames acquired consecutively for a total of 4 min; at the same time, arterial blood samples were acquired from the abdominal aorta by a catheter advanced through the femoral artery.

Human Hepatic Studies

A total of eight dynamic, ^{13}N-ammonia hepatic PET studies were performed on four healthy male human volunteers and four male patients with a history of myocardial infarction (*20*). About 20 mCi of ^{13}N-ammonia were injected intravenously over 30 sec, for each study. The scan protocol for the ECAT 931/08 whole-body PET scanner consisted of twelve 10-sec frames and six 20-sec frames acquired consecutively (a total of 4 min) with the axial FOV including the heart and the superior aspect of the liver. No blood samples were acquired.

Image Acquisition

All sinograms were corrected online for attenuation, geometric mispositioning (*21*) and deadtime (*22*). All images were reconstructed by filtered backprojection using a Shepp-Logan filter with cutoff set at 30% of the Nyquist frequency (Ny) of the

system, or 0.159 mm^{-1}. This filter/cutoff combination is routinely used for cardiac PET studies performed at our institution, having been qualitatively determined to achieve optimal tradeoff between image resolution and uniformity. However, it is worth stressing that the approach described will work for any filter and cutoff, since the resulting transaxial resolution is accounted for in Equations 3 and 4. The system's transaxial resolution corresponding to the Shepp-Logan filter at 30% Ny cutoff is 10.85 mm FWHM as measured with a standard line source of activity, and it is relatively independent of the line source's position within the transaxial FOV (Fig. 1). Zoom factors resulting in ca. 1 mm/pixel (canine renal studies) and 2 mm/pixel (human hepatic studies) in 256 × 256 images were used in the reconstruction process, so as to adequately sample the abdominal aorta.

Image Processing

In the canine renal studies, several rectangular ROIs (each 2–3 mm by side) were drawn over the renal cortex, and the various renal time activity curves calculated. Every curve was corrected for partial volume effects in the kidney through division by an appropriate recovery coefficient, which was determined with the automated software package Explorer® on a Macintosh IIcx computer (*17*). In essence, the recovery coefficient for the kidney cortex is determined by dividing the cortex into adjacent sectors. Each sector is then treated as a one-dimensional infinite bar of thickness 2R. Explorer automatically estimates the average sector emiwidth R, sector by sector, by fitting several profiles through each sector. The estimates of R are then used with Equation 4 to estimate the recovery coefficients for the various sectors, and each renal time-activity curve is corrected according to the sector it lies in. The approach described is identical to that routinely used to estimate the recovery coefficient of the myocardial wall in cardiac studies (*16,18*). The decision to use the same procedure was based on the fact that ^{13}N-ammonia concentrates in the renal cortex during the initial 90–120 sec from injection, yielding an annular activity distribution similar to that seen in the myocardium. A square ROI (4 to 9 mm^2) was also drawn over the abdominal aorta on one plane, generally a few cm higher than the plane of the renal cortex ROIs, to generate the arterial input function. This ROI was centered on the pixel of maximum activity in the aorta, which coincided with the center of the aorta's section in the image plane.

In the human hepatic studies, a 4-mm square ROI was drawn over the abdominal aorta on one plane and a slightly larger rectangular ROI over the LVC on another plane, thus generating two distinct input functions. One ROI was also drawn over the liver, and the relative time-activity curve (TAC) calculated. The dynamic frame and image plane selection was similar to that in canine renal studies. The LVC input function and liver tissue curves were not corrected for partial volume effects since both the LVC and the liver are large compared to the scanner's transaxial resolution.

A typical sequence of canine renal images obtained 20–40 sec after the injection of a bolus of ^{13}N-ammonia is shown in Figure 3. Estimation of the aorta diameter was performed on the dynamic frame in which the aorta showed greatest contrast relative to the surrounding structures. The image plane utilized was at the level of the superior aspect of the left kidney. In that plane and for that optimal dynamic frame, activity along a line connecting the aorta to either renal cortices fell to less than 10% of the maximum activity in the aorta, showing that the latter was reasonably separated from the renal cortices. Thus, no reslicing was needed.

Using PET analysis software developed in our laboratory, a circular ROI was centered over the aorta section, and the roundness of the latter was visually evaluated by varying the ROI's radius until its circle reached the aorta's perceived boundary in any direction. In six of eight studies, the abdominal aorta boundary and the ROI circle overlapped, which was judged to be a good indicator of the aorta's perpendicularity to the image plane. In the remaining two studies, the aorta's section proved elliptical by exceeding the ROI circle along a preferential direction. Such direction defined the long axis of the ellipse, and the activity profile was calculated along the short axis of the ellipse. Since our PET analysis software allows the calculation of horizontal or vertical profiles, the image was rotated by an appropriate angle to bring that short axis in the horizontal or vertical position. The activity profile, measured from a strip 1 pixel wide in the image, was used as P(x) in Equation 4 to estimate the actual diameter 2R of the aorta in the plane considered. R was used with Equation 2 to estimate the recovery coefficient RC_{aorta}, the inverse of which was multiplied by the activity values determined from ROI analysis.

Human liver images were noisier due to the relatively low hepatic arterial blood flow, as shown in the dynamic sequence of Figure 4. On the other hand, such low flow caused little spillover into the aorta from the adjacent tissue, so no spillover correction was applied. Again, estimation of the aorta diameter was performed on the dynamic frame in which the aorta showed greatest contrast relative to the surrounding structures, and processing was identical to the renal studies.

RESULTS

Comparison Between PET Abdominal Aortic and Arterial Blood Input Function

In the canine renal studies, PET abdominal aortic blood-pool data, after correction for partial volume effects, were compared to the arterial blood samples. Figure 5 qualitatively shows the good agreement in shape and magnitude between a pair of input functions, for a typical ^{13}N-ammonia renal study. Only the first 90–120 sec of the dynamic data were used for the calculation of regional renal blood flow (rRBF), so as to minimize contamination by plasma metabolites (*19*); accordingly, a quantitative comparison between the two sets of integrals for the various input function pairs from 0 to 90–120 sec was performed. The results are shown in Figure 6, with linear regression demonstrating excellent agreement between the two methods with a slope nearly equal to 1.0 (slope = 1.03 ± 0.09; $R^2 > 0.95$, $p < 0.001$). The final estimate for the average aorta diameter, as obtained from activity profiles across the aorta and Equation 4, was 12.6 ± 1.1 mm, while the average recovery coefficient, as determined from Equation 2, was 60.3% ± 6.4%.

While comparing the shape and magnitude of the two input functions yields valuable information as to whether this technique (abdominal aorta) is consistent with the commonly accepted gold standard (arterial sampling), it is also important to compare the parameter estimates from

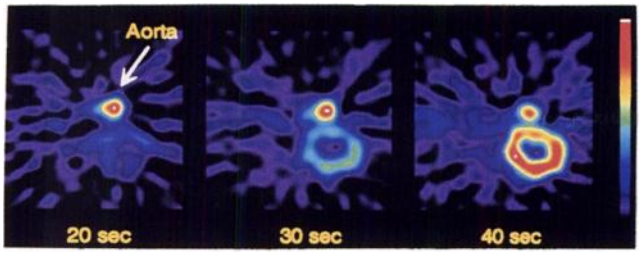

FIGURE 3. Ten-second PET images obtained 20, 30, and 40 sec after injection of a 10-mCi bolus of ^{13}N-ammonia in an anesthetized mongrel dog. A Shepp-Logan filter with cutoff of 30% of the Nyquist frequency of the system was used in reconstruction. Note that the simultaneous presence of blood-pool activity and tissue uptake might pose spillover problems. To minimize such effect, aortic analysis was performed in the image plane at the level of the superior third of the left kidney, shown in this figure.

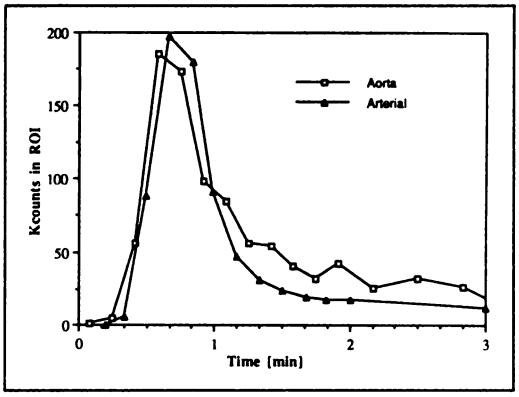

FIGURE 5. Typical blood-pool time-activity curves (input functions) determined by (a) ROI measurements of abdominal aortic activity from dynamic PET images and (b) well counter measurements of arterial blood samples withdrawn at regular intervals, in an anesthetized mongrel dog injected with a 10-mCi bolus of ^{13}N-ammonia.

those input functions and mathematical modeling. For this set of experiments, it was decided to compare the estimates of rRBF obtained using the PET abdominal aortic data to those obtained using arterial blood sampling. The two-compartment, ^{13}N-ammonia tracer-kinetic model used (Fig. 7) consists of both a free space, composed of vascular and free ammonia, and a trapped space for ^{13}N bound in tissue. The differential equations governing the model are:

$$\frac{dQf(t)}{dt} = \frac{-(K1 + F)\cdot Qf(t)}{V} + k2\cdot Qt(t) + F\cdot Ca(t)\cdot p \qquad \text{Eq. 7}$$

$$\frac{dQt(t)}{dt} = \frac{K1\cdot Qf(t)}{V} - k2\cdot Qt(t), \qquad \text{Eq. 8}$$

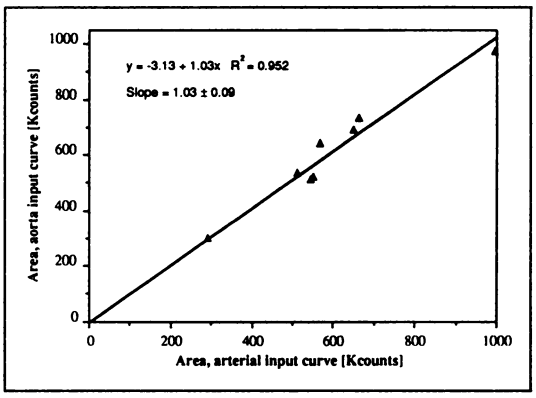

FIGURE 6. Correlation between the integrals from 0 to 90–120 sec of the various input functions pairs (one pair is shown in Fig. 5) for the eight renal studies performed on mongrel dogs.

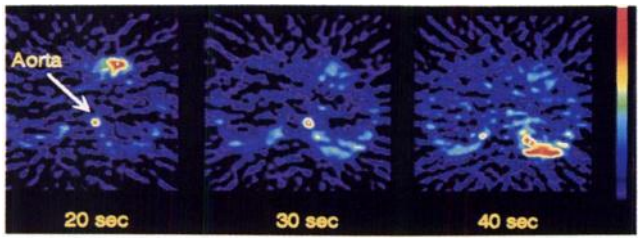

FIGURE 4. Ten-second PET images obtained 20, 30, ad 40 sec after injection of a 20-mCi bolus of ^{13}N-ammonia in a healthy human volunteer. A Shepp-Logan filter with cutoff of 30% of the Nyquist frequency of the system was used in reconstruction. Note the increased image noise compared to Figure 3, due to the relatively low hepatic arterial flow. Also, note the concentration of radioactivity in the left ventricular cavity, anterior to the aorta (particularly evident in the leftmost image) and in the spleen, right posterior lateral to the aorta (especially in the rightmost image).

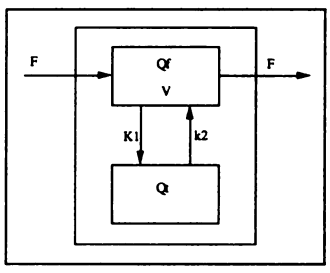

FIGURE 7. Two-compartment model utilized to calculate the rRBF in canine renal studies and the rHABF in human hepatic studies. Q(t) is the total activity (cpm/pixel) in the free (Qf) and trapped (Qt) space, K1 is the forward rate constant from free to trapped compartment (ml/min/g), k2 the reverse-rate constant from trapped to free compartment (min^{-1}), and V is the distribution volume of the tracer within the free space (ml/g).

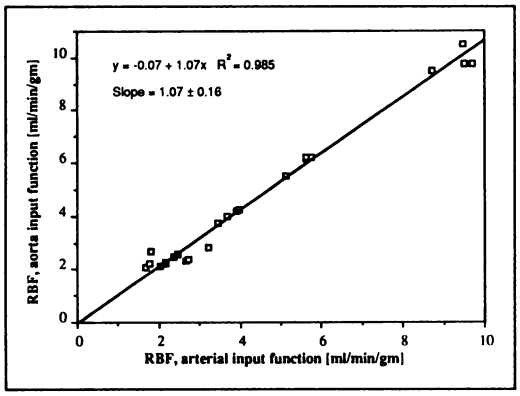

FIGURE 8. Correlation between the rRBF values calculated using the two different determinations of the input fraction (PET abdominal aortic data and blood samples) and the model of Figure 7 in canine renal studies.

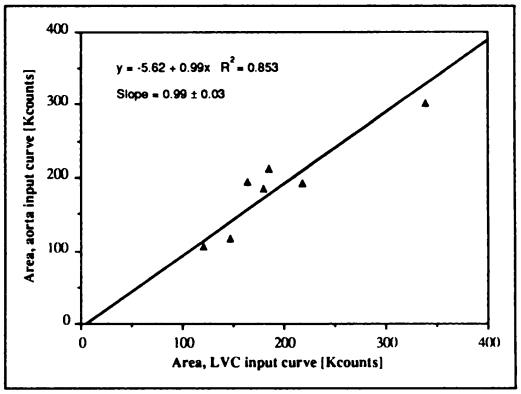

FIGURE 10. Correlation between the integrals from 0 to 90–120 sec of the various input functions pairs (one pair is shown in Fig. 9) for the eight hepatic studies performed on human subjects.

where Qf(t) and Qt(t) represent total activity in the free and trapped space, K1 is the forward-rate constant from the free to trapped compartment, k2 is the reverse-rate constant from the trapped to free compartment, V is the distribution volume of the tracer within the free space, F is rRBF, Ca(t) the arterial input function, and p the specific gravity of blood.

The tracer kinetic modeling software BLD (*23*) was used to perform all non-linear fitting of the model equations to the initial 90–120 sec of the time-activity data. A comparison of the estimates of rRBF based on abdominal aorta PET and on arterial blood sampling data is shown in Figure 8, and linear regression again demonstrates good agreement between the two methods (slope = 1.07 ± 0.16; $R^2 > 0.98$, $p < 0.001$).

Comparison Between PET Abdominal Aortic and PET LVC Input Function

In the human hepatic studies, the PET abdominal aortic blood-pool data were corrected for partial volume effects and compared to the blood-pool data obtained from PET images of the LVC. Figure 9 qualitatively shows the good agreement in shape and magnitude between the input functions calculated from PET abdominal aorta and LVC, for a typical ^{13}N ammonia study. Only the first 90–120 sec of the dynamic data were used for the calculation of the regional hepatic arterial blood flow (rHABF), so as to minimize contamination by plasma metabolites and portal venous return of ^{13}N (*20*). Accordingly, a quantitative comparison between the two sets of integrals for the various input function pairs from 0 to 90–120 sec was performed. The results are shown in Figure 10, with linear regression analysis demonstrating very good agreement between the two methods (slope = 0.99 ± 0.03; $R^2 > 0.85$, $p < 0.001$). The final estimate for the average aorta diameter, as calculated from an activity profile across the aorta and Equation 4, was 16.7 ± 1.7 mm, while the average recovery coefficient, as determined from Equation 2, was 79.6% ± 5.9%.

The estimates of rHABF obtained using the PET abdominal aortic data were compared to those obtained using PET LVC data. The two-compartment, ^{13}N-ammonia tracer-kinetic model used was the same as that for the

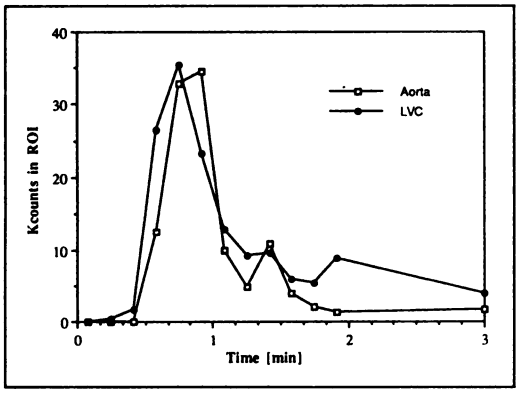

FIGURE 9. Typical blood-pool time-activity curves determined by (a) ROI measurements of abdominal aortic activity and (b) ROI measurements of LVC activity from dynamic PET images, in a healthy human volunteer injected with a 20-mCi bolus of ^{13}N-ammonia.

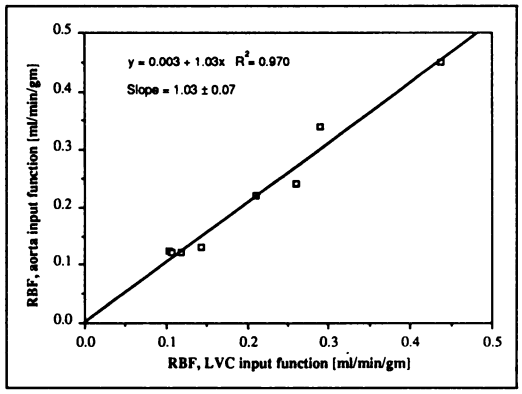

FIGURE 11. Correlation between the rHABF values calculated using the two different determinations of the input function (PET abdominal aortic and LVC data), and the model of Figure 7 in human hepatic studies.

canine renal studies (Fig. 7), with F now representing rHABF. A comparison of the estimates of rHABF based on abdominal aorta and on LVC PET data is shown in Figure 11, and linear regression analysis demonstrates the good agreement between the two methods (slope = 1.03 ± 0.07; $R^2 = 0.97$, $p < 0.001$).

DISCUSSION AND CONCLUSIONS

The advancements in whole-body PET imaging (*24*) and the increasing axial FOV of current PET scanners (*25*) encourage the investigation of various intra-abdominal organs, including the liver and kidneys. An important requirement for quantitative analysis in clinical hepatic and renal PET imaging is a fast and noninvasive PET measurement of the input function from transaxial PET images. We have found that estimating the input function from ROI analysis of dynamic PET images containing the abdominal aorta is possible and accurate, if one can reliably correct for partial volume effects due to the aorta's size.

In practice, the aortic recovery coefficient depends not only on the actual aorta size, but also on the intrinsic resolution of the PET scanner, as well as on the type and cutoff frequency of the filter used in reconstruction. Thus, we have developed a method that makes use of activity profiles across the abdominal aorta to estimate its diameter as a function of the scanner's image resolution. The aorta diameter information is then used to calculate the recovery coefficient to be applied to the ROI measurements under the hypothesis that the aorta's section in the image plane is circular.

Validation of this new methodology involved comparing the corrected abdominal aortic input functions, their integrals from 0 to 90–120 sec and the values of regional blood flow calculated by them, with the corresponding values obtained from PET LVC analysis (human hepatic studies) and arterial sampling (canine renal studies). In all cases, good to excellent correlation resulted.

To further validate the technique, the estimates of aortic diameters from PET images were compared to direct measurements obtained from renal angiograms. In three human subjects studied with both PET imaging and renal angiography, the abdominal aortic diameters at the level superior to the right kidney from PET images were 17.1 mm, 16.9 mm and 17.9 mm, and from angiograms were 17.5 mm, 16.7 mm and 18.3 mm, respectively. Even though the sample size is small, the above preliminary results show good correlation of the diameter estimates with direct angiographic measurements.

Spillover of activity into the abdominal aorta from surrounding structures can be a problem when (a) those structures have high concentration of radioactivity, or (b) when the resolution of the system is low because low cutoff frequencies are used in the reconstruction process. Both of these conditions are present in our canine renal studies, so some spillover from the renal cortices into the aorta may occur in spite of selecting a relatively high image plane for the aorta ROI analysis. Moreover, radiation scattered into the abdominal aorta from the renal cortices or other structures containing radioactivity will also contribute counts to the aortic ROI, artificially enhancing the aortic input function. The relative error due to scatter is inversely proportional to the activity concentration ratio between the aorta and the other structures in the FOV. The slight overestimation of activity (relative to the arterial curve) in the late frames of the abdominal aortic curve in Figure 5, for instance, could lead to errors if more than the initial 90 sec of data were utilized. One should consider, however, that some error due to myocardial spillover is present in PET LVC data as well, a possible example is the LVC curve in Figure 9. By comparison, the abdominal aortic curve in the same figure shows no sign of overestimation due to spillover, as is understandable given the relatively low radioactivity concentration in the hepatic tissue.

In conclusion, determination of the input function from the abdominal aorta in patients and animals is possible and leads to results comparable to those obtained from other widely used methods, if appropriate corrections for the partial volume effect are applied. While some errors are expected due to spillover, the benefits from having a clinically usable, fast and noninvasive procedure which does not depend on calibration or conversion factors between PET and well counter data would suggest that this procedure be routinely used in clinical hepatic and renal dynamic PET studies. Future tomographs with larger axial FOV (15–20 cm) will ideally enable one to acquire image slices where the abdominal aorta is the only structure containing radioactivity, thus virtually eliminating spillover problems.

It must be remembered that this procedure has been validated for short duration dynamic PET studies using ^{13}N-ammonia, a case in which the activity in the abdominal aorta is high and good contrast with the surrounding structures results. For longer duration studies (such as with FDG), background activity may be significantly higher than that in the aorta, thus causing large errors in the measured aortic input function in the later phases of the study. In cases like these, our approach may need to be modified and its effectiveness re-evaluated.

ACKNOWLEDGMENTS

The authors wish to thank Herb Hansen for his help with the animal experiments, and Ron Sumida, Larry Pang, Gloria Stocks and Judy Edwards for their assistance with isotope scheduling and delivery. This work was supported in part by Department of Energy contract DE-FCO3-87ER60615 and National Institutes of Health grants HL33177 and HL2202-2.

REFERENCES

1. Huang SC, Phelps ME. Principles of tracer kinetic modeling in positron emission tomography and autoradiography. In: ME Phelps, JC Mazziotta, HR Schelbert ed. *Positron emission tomography and autoradiography. Principles and applications for the brain and heart.* New York: Raven Press,

1986:287–346.
2. Di Chiro G, Brooks RA. PET quantitation: blessing and curse. *J Nucl Med* 1988;29:1603–1604.
3. Weinberg IN, Huang SC, Hoffman EJ, et al. Validation of PET-acquired input functions for cardiac studies. *J Nucl Med* 1988;29:241–247.
4. Gambhir SS, Huang SC, Digby WM, Schelbert HR, Phelps ME. A new method for partial volume and spillover correction in cardiac PET scans. *J Nucl Med* 1989;30:824–825.
5. Rajeswaran S, Bailey D, Hume S, Jones T, Townsend D. 2D and 3D imaging of small animals and the human radial artery with a high resolution detector for PET. *Conference Record of the 1990 IEEE Nuclear Science Symposium, volume II.* 1990:1308–1312.
6. Chen BC, Huang SC, Hawkins RA, et al. Non-invasive quantification of regional hepatic and renal blood flow with N-13 ammonia, dynamic PET and a two-compartmental model [Abstract]. *Clin Nucl Med* 1990;15:764.
7. Shelton ME, Green MA, Mathias CJ, et al. Assessment of regional myocardial and renal blood flow with copper-PTSM and PET. *Circulation* 1990;82:990–997.
8. Smith JJ. Role of positron emission tomographic scanning in the diagnosis of liver disease. *Semin Liver Dis* 1989;91:86–89.
9. Tamaki N, Rabito CA, Alpert NM, et al. Serial analysis of renal blood flow by positron tomography with rubidium-82. *Am J Physiol (Heart Circ Physiol)* 1986;20:H1024–1030.
10. Ohtake T, Yokohama I, Masuo M. Noninvasive quantification method for measuring glucose utilization of thoracic and abdominal organs [Abstract]. *J Nucl Med* 1990;31:778.
11. Hoffman EJ, Huang SC, Phelps ME. Quantitation in positron emission tomography. 1. Effect of object size. *J Comput Assist Tomogr* 1979;3:299–308.
12. Derenzo SE, Huesman RH, Cahoon JL, et al. A positron tomograph with 600 BGO crystals and 2.6 mm resolution. *IEEE Trans Nucl Sci* 1988;35:659–664.
13. Digby WM, Hoffman EJ, Phelps ME, Williams CW, Moyer JA, Casey ME. A multiplane high-resolution PET system for animal studies [Abstract]. *J Cereb Blood Flow Metab* 1989;9:236.
14. Henze E, Huang SC, Ratib O, Hoffman EJ, Phelps ME, Schelbert HR. Measurements of regional tissue and blood-pool radiotracer concentrations from serial tomographic images of the heart. *J Nucl Med* 1983;24:987–996.
15. Burton AC. Relation of structure to function of the tissues of the wall of blood vessels. *Phys Rev* 1954;34:619–642.
16. Kuhle W, Porenta G, Buxton D, et al. Quantification of regional myocardial blood flow using N-13-ammonia and reoriented dynamic PET imaging. *J Nucl Med* 1991;32:909–910.
17. Ratib O, Huang HK. CALIPSO: an interactive software package for multimodality medical image analysis on a personal computer. *J Med Im* 1989;3:205–216.
18. Gambhir S. Quantitation of the physical factors affecting the tracer kinetic modeling of cardiac positron emission tomography data. Ph.D. Dissertation, University of California at Los Angeles, 1990.
19. Chen BC, Germano G, Huang SC, et al. A noninvasive method for quantification of renal blood flow with N-13-ammonia, dynamic positron emission tomography and a two-compartment model [Abstract]. *J Nucl Med* 1991;32:953.
20. Chen BC, Huang SC, Germano G, et al. Noninvasive quantification of hepatic arterial blood flow with N-13-ammonia and dynamic positron emission tomography. *J Nucl Med* 1991;32:2199–2208.
21. Hoffman EJ, Guerrero TM, Germano G, Digby WM, Dahlbom M. PET system calibration and corrections for quantitative and spatially accurate images. *IEEE Trans Nucl Sci* 1989;36:1108–1112.
22. Germano G, Hoffman EJ. Correction for deadtime loss in PET systems that employ 2-D modular detectors [Abstract]. *J Nucl Med* 1990;31:864.
23. Carson RE, Huang SC, Phelps ME. BLD, a software system for physiological data handling and data analysis. *Proceedings of the fifth annual symposium on computer applications in medical care.* New York: IEEE; 1981:562–565.
24. Guerrero TM, Hoffman EJ, Dahlbom M, Cutler PD, Hawkins RA, Phelps ME. Characterization of a whole body imaging technique for PET. *IEEE Trans Nucl Sci* 1990;37:676–680.
25. ECAT and NeuroECAT user's manual. CTI Inc., Knoxville, TN, 1986.

EDITORIAL

A Bloody Future for Clinical PET?

During the past few years, PET imaging has emerged as a clinical tool because of its great potential for high quality imaging.

The uniqueness of PET lies in the fact that it is capable of quantitative regional measurement of physiological parameters. A number of general factors contribute to its quantitative nature. These include the unique physical properties of coincidence imaging, which allow for the absolute measurement of activity concentrations, the availability of short-lived positron-emitting isotopes which can easily be incorporated into biologically molecules, and the ability, by using ancillary information such as radioactivity concentrations of labeled substances in the arterial blood, to estimate regional physiological parameters. The first of these factors is intrinsic to modern PET instrumentation and the second is widely exploited in PET radiochemistry as it is practiced today.

It is the third area, however, that is often ignored in emerging clinical PET studies. It is widely believed, with some justification perhaps, that the insertion of arterial lines and the subsequent collection and processing of arterial blood is not compatible with the practice of clinical PET. Practitioners argue that arterial blood sampling limits patient throughput, requires extra personnel and processing time, exposes the patient to the unnecessary risks associated with the insertion of an arterial line and exposes personnel to the risks associated with the handling of patient blood.

With the increase in clinical PET studies during the past few years, imaging alone without the use of arterial blood concentration data is beginning to be used almost exclusively in many centers. This may be a trend which limits the long-term applicability of PET. It is not entirely clear that this trend should be encouraged. There is no question that, if arterial sampling could be eliminated with only minor constraints on the applicability of the technique, we would all readily throw away our catheters. But is this a realistic goal?

Because of the desire to eliminate the burdens of arterial sampling, a number of schemes to obtain input function data have been evaluated. In the past, these have included attempts to measure signals from the cardiac

Received Feb. 5, 1992; accepted Feb. 5, 1992.
For reprints contact: John Correia, PhD, Department of Radiological Sciences, Massachusetts General Hospital, Edwards Research Bldg., Fruit St., Boston, MA 02114.